Journal of Applied Physics

Heavily *n*-doped Ge: Low-temperature magnetoresistance properties on the metallic side of the metal–nonmetal transition

Cite as: J. Appl. Phys. **127**, 045705 (2020); https://doi.org/10.1063/1.5125882
Submitted: 28 August 2019 . Accepted: 15 January 2020 . Published Online: 30 January 2020

A. Ferreira da Silva, M. A. Toloza Sandoval, A. Levine, E. Levinson, H. Boudinov, and B. E. Sernelius

ARTICLES YOU MAY BE INTERESTED IN

Multiferroic behavior from synergetic response of multiple ordering parameters in $BiFeO_3$ single crystal under high magnetic field up to 50 Tesla
Journal of Applied Physics **127**, 044101 (2020); https://doi.org/10.1063/1.5131411

Improving the performance of light-emitting diodes via plasmonic-based strategies
Journal of Applied Physics **127**, 040901 (2020); https://doi.org/10.1063/1.5129365

Identification of the donor and acceptor states of the bond-centered hydrogen-carbon pair in Si and diluted SiGe alloys
Journal of Applied Physics **127**, 045701 (2020); https://doi.org/10.1063/1.5135757

Your Qubits. Measured.
Meet the next generation of quantum analyzers
- Readout for up to 64 qubits
- Operation at up to 8.5 GHz, mixer-calibration-free
- Signal optimization with minimal latency

Find out more

© 2020 Author(s).

Heavily *n*-doped Ge: Low-temperature magnetoresistance properties on the metallic side of the metal–nonmetal transition

Cite as: J. Appl. Phys. **127**, 045705 (2020); doi: 10.1063/1.5125882
Submitted: 28 August 2019 · Accepted: 15 January 2020 ·
Published Online: 30 January 2020

View Online

Export Citation

CrossMark

A. Ferreira da Silva,[1,2,a)] M. A. Toloza Sandoval,[1] A. Levine,[3] E. Levinson,[3] H. Boudinov,[4] and B. E. Sernelius[5]

AFFILIATIONS

[1] Instituto de Física, Universidade Federal da Bahia, 40210-340 Salvador, Bahia, Brazil
[2] Instituto de Física, Universidade de São Paulo, Laboratório de Cristais Iônicos, Filmes Finos e Datação, 05508-090 Butantã, São Paulo, Brazil
[3] Instituto de Física, Universidade de São Paulo, Laboratório de Novos Materiais Semicondutores, 05508-090 Butantã, São Paulo, Brazil
[4] Instituto de Física, Universidade Federal do Rio Grande do Sul, 91501 970 Porto Alegre, Rio Grande do Sul, Brazil
[5] Division of Theory and Modeling, Department of Physics, Chemistry and Biology, Linköping University, SE-581 83 Linköping, Sweden

[a)] **Author to whom correspondence should be addressed:** ferreira.fis@gmail.com

ABSTRACT

We report here an experimental and theoretical study on the magnetoresistance properties of heavily phosphorous doped germanium on the metallic side of the metal–nonmetal transition. An anomalous regime, formed by negative values of the magnetoresistance, was observed by performing low-temperature measurements and explained within the generalized Drude model, due to the many-body effects. It reveals a key mechanism behind the magnetoresistance properties at low temperatures and, therefore, constitutes a path to its manipulation in such materials of great interest in fundamental physics and technological applications.

Published under license by AIP Publishing. https://doi.org/10.1063/1.5125882

I. INTRODUCTION

The advent of doped semiconductors stands as a milestone in the development of semiconductor devices. Since the seminals, with p-n junction transistors[1] and solar cells,[2] until the current trends, with midinfrared sensors and plasmonic devices,[3] doped semiconductors have provided a fertile ground for fundamental research and applied physics. Among the possibilities, such materials can be used in energy-efficient windows,[4,5] because they can act as a metal for low photon energies and as a semiconductor (or insulator) for high photon energies. In comparison with ordinary metals, for which the carrier densities are discrete and limited to a narrow range, doped semiconductors constitute more flexible systems, allowing a continuous variation of the carrier concentration over a wide range.[6] In particular, such flexibility is even larger in *n*-doped many-valley semiconductors, like Si and Ge. On the one hand, Si has six equivalent band minima in the $\langle 100\rangle$-directions within the Brillouin zone (BZ); on the other, Ge has eight in the L-points (the intersection of the $\langle 111\rangle$-directions with the zone faces). Since the conduction-band valleys are strongly anisotropic, when electrons are filling up the states at the bottom of the conduction-band minima, they do not form Fermi spheres but cigar-shaped Fermi ellipsoids. As a consequence, the contribution to transport and optical properties from each Fermi volume is anisotropic. However, the sum of contributions from all volumes is isotropic since the overall symmetry is cubic; note that while Si has six Fermi ellipsoids in the BZ, in Ge the eight minima lie at the BZ boundary, leading to electrons effectively distributed within four Fermi ellipsoids.

It is well known that the application of uniaxial stress on the sample breaks the afore-described symmetry, such that part of the minima move upward in energy and part move downward, depending on the applied stress direction. There is a redistribution of electrons between the valleys and the applied stress results in piezoresistance[7,8] and optical birefringence.[8,9] Furthermore, it is also possible

Published under license by AIP Publishing.

to modify the distribution of electrons by using an external magnetic field. Each of the (aforementioned) Fermi volumes is doubly degenerate and corresponds to spin-up and spin-down electrons. With the introduction of a magnetic field, the spin-up valleys move up in energy and the spin-down valleys move down—i.e., there is a redistribution of electrons where the Fermi level is the same for both valley types. The system remains isotropic, but important transport properties change, in particular, the electric current parallel to the magnetic field, which is expressed in terms of the longitudinal magnetoresistance, as will be here discussed in detail.

For all conducting pure single crystals, the acquired knowledge shows that, in general, the resistivity increases with the applied magnetic field, i.e., the magnetoresistance is positive. On the other hand, doped semiconductors require a detailed description at the critical concentration, n_c, when the system turns metallic. For densities much larger than n_c, if we place the donor electrons at the bottom of the host conduction band and treat them as a noninteracting electron gas, we found an unambiguous agreement with experiments. However, an anomalous regime arises when n approaches n_c, in which, for example, the heat capacity[10] and the spin susceptibility[11,12] are enhanced. In particular, low-temperature magnetotransport properties are critically affected by this regime, being the negative magnetoresistance a critical signature. These so-called anomalies have attracted much attention with several models reported in the literature.[13–22] With a peculiar interpretation, Sernelius and Berggren[23] proposed that the donor electrons end up in the conduction band of the host already at the critical concentration n_c and suggested that the anomalous properties, on the metallic side of and close to the transition point, are caused by the many-body effects.[24] One step forward, we explore here such anomalous behavior of the magnetoresistance in heavily n-doped Ge, comparing results from low-temperature magnetotransport measurements with those obtained from the theory.

II. MEASUREMENTS AND SAMPLES

As illustrated in Fig. 1, Hall and longitudinal resistance measurements were performed in an Oxford cryostat with VTI (Variable Temperature Insert), under a perpendicular magnetic field provided by a superconducting coil. To prevent heating effect and provide a clear signal for our measurements, the lock-in technique was employed with frequencies 0.5–13 Hz in the temperature range of 1.5–4.2 K and bias current of $10\,\mu$A.

The samples were prepared in the following way: P-type, Ga doped (100)-oriented square, $7 \times 7\,\text{mm}^2$, Ge samples with resistivity in the range of $1-10\,\Omega$cm were implanted with phosphorus at room temperature. In each sample, implantations with energies of 240, 140, 80, 40, and 20 keV were accumulated with appropriate doses to obtain a plateaulike profile of P, from the surface to the depth of about $0.40\,\mu$m, according to TRIM code simulation.[25] In Fig. 2, we show the simulation for the concentration profile. To achieve a P atomic concentration of $1 \times 10^{18}\,\text{cm}^{-3}$, the implanted P doses were $2.0 \times 10^{13}\,\text{cm}^{-2}$ (at 240 keV), $6.0 \times 10^{12}\,\text{cm}^{-2}$ (at 140 keV), $4.0 \times 10^{12}\,\text{cm}^{-2}$ (at 80 keV), $2.0 \times 10^{12}\,\text{cm}^{-2}$ (at 40 keV), and $1.1 \times 10^{12}\,\text{cm}^{-2}$ (at 20 keV). The doses in the other samples were scaled to this sample, according to the ratio of the desired P

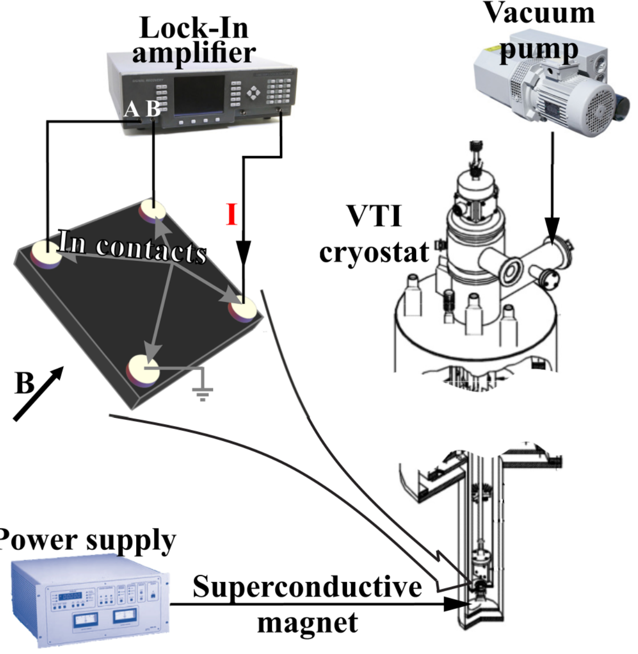

FIG. 1. Measurement setup consists of a VTI (Variable Temperature Insert) cryostat with the superconductive magnet, Lock-In amplifier, and pump. GeP sample has four In contacts arranged in a Van der Paw geometry located at the corners of $7 \times 7\,\text{mm}^2$ square. Magnetotransport measurements are done by the conventional Lock-In technique with signal recovery (Model 7280) DSP dual phase amplifier, which has a high input impedance of 100 MΩ. The sample was located in the superconductive magnet (Oxford) with the perpendicular to its surface magnetic field up to 5 T. Mechanical pump allowed us to reach temperatures down to 1.5 K.

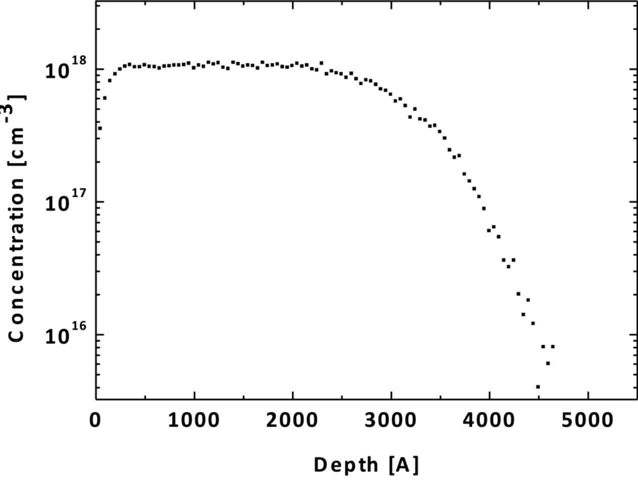

FIG. 2. Simulated multiple implantation phosphorous profile for a nominal sample atomic concentration of $10^{18}\,\text{cm}^{-3}$. The implanted P^+ doses were $2.0 \times 10^{13}\,\text{cm}^{-2}$ (at 240 keV), $6.0 \times 10^{12}\,\text{cm}^{-2}$ (at 140 keV), $4.0 \times 10^{12}\,\text{cm}^{-2}$ (at 80 keV), $2.0 \times 10^{12}\,\text{cm}^{-2}$ (at 40 keV), and $1.1 \times 10^{12}\,\text{cm}^{-2}$ (at 20 keV).

Published under license by AIP Publishing.

concentration. Furthermore, the damage annealing and the electrical activation of P were performed at 600 C for 1 min in argon atmosphere in a Rapid Thermal Annealing furnace to avoid high thermal budget; Van der Pauw structures[26] were fabricated by applied indium contacts at the corners of the samples and annealing at 80 °C on a hot plate for 1 min was performed to improve the contacts. The implantation process is described in Refs. 27–29.

III. THEORETICAL APPROACH

From the theoretical point of view, the conduction band of Ge has four equivalent valleys ($\nu = 4$); there are eight minima in the $(\pm 1, \pm 1, \pm 1)/\sqrt{3}$ directions, but they all are on the zone boundary so only half of each cigar-shaped Fermi volume is inside the Brillouin zone. In heavily n-type doped germanium, on the metallic side of the metal–nonmetal transition (i.e., $n > n_c$), the donor electrons are up in the conduction-band valleys. We consider that the electrons are distributed in ν Fermi spheres and neglect some known anisotropy effects on the resistivity;[30] the relation between the radius of each sphere is then given as[29] $k_0 = (3\pi^2 n/\nu)^{1/3}$ and the Fermi energy given by $E_0 = \hbar^2 k_0^2/(2m) = \hbar^2 k_0^2/(2m_{de} m_e)$, where m_e is the electron rest mass and $m_{de} = 0.22$ is the effective mass of the density of states in one valley of the conduction band. In particular, the contributions from the exchange and correlation energy, E_{xc}, due to the influence of ionized-donor potentials (the band structure energy, E_b), affect the parabolic band dispersion and the density of states. Our model starts from the density of states from one valley, i.e.,

$$D_E = D_k/[dE(k)/dk] = \frac{k^2}{\pi^2 [dE(k)/dk]}, \tag{1}$$

and take into account that in each valley there are two states for each $\mathbf{k}$ (i.e., one for each spin, up and down). Since $D_E^0 = km/\pi^2\hbar^2$ is the density of states for noninteracting electrons, the density of states for interacting electrons can be expressed, in analogy, by introducing a wave-number dependent effective mass, i.e.,

$$D_E = km^*/\pi^2\hbar^2, \tag{2}$$

with the effective mass given by

$$m^*(k) = m/[1 - \beta(k)], \tag{3}$$

where $\beta(k)$ gets a contribution from each of the interaction energies, $\beta(k) = \beta_{xc}(k) + \beta_b(k)$, such that

$$\beta_{xc}(k) = -\frac{m}{\pi^2 k}\frac{\partial}{\partial k}\frac{\delta N \cdot E_{xc}}{\delta n(\mathbf{k})}, \quad \beta_b(k) = -\frac{m}{\pi^2 k}\frac{\partial}{\partial k}\frac{\delta N \cdot E_b}{\delta n(\mathbf{k})}. \tag{4}$$

Here, N is the total number of electrons and $n(\mathbf{k})$ is the occupation number of the state with wave-vector $\mathbf{k}$. Specially important for this paper, one effect of the interactions is that around the Fermi level the effective mass and density of states are enhanced.[31]

We use the generalized Drude model[32,33] to calculate the resistivity. For the static case, as here, the results agree with the so-called Ziman's formula,[34]

$$\rho = \frac{1}{ne^2\tau/m^*}, \qquad \frac{1}{\tau} = \frac{4}{3}\frac{\nu e^4 m}{\pi\hbar^3\kappa^2}\int_0^{2k_0} dq \frac{1}{q\tilde{\varepsilon}^2(q,0)}, \tag{5}$$

where ρ, τ, and κ are, respectively, resistivity, transport time, and dielectric constant ($\kappa = 15.36$ for Ge).

The presence of a static and spatially homogeneous magnetic field $\mathbf{B}$ leads to a redistribution of electrons between spin-up and spin-down bands, which affects the density of states, the effective mass at the Fermi level, the conductivity and the transport time. Let us introduce the spin-polarization parameter, s, that varies from zero in the absence of $\mathbf{B}$ to 1 at full polarization (all electrons have spin down),

$$s = \frac{n^\downarrow - n^\uparrow}{n}. \tag{6}$$

For spin-up and spin-down electrons, the density and Fermi wave-number are, respectively,

$$n^\uparrow = n(1 - s)/2, \quad n^\downarrow = n(1 + s)/2, \quad k_0{}^\uparrow = k_0(1 - s)^{1/3}, \quad k_0{}^\downarrow = k_0(1 + s)^{1/3}. \tag{7}$$

Therefore, the resistivity is now written as[29]

$$\rho(s) = \frac{m/e^2}{n^\uparrow\tau^\uparrow(1 - \beta^\uparrow) + n^\downarrow\tau^\downarrow(1 - \beta^\downarrow)}. \tag{8}$$

Note that the magnetoresistance is given by $\Delta\rho/\rho = [\rho(s) - \rho(0)]/\rho(0)$, i.e., it is a function of the spin polarization s; however, the experimental results are given in terms of B. When the modulus of the magnetic field is small enough, one can assume the following linear relation between B and s:

$$B[T] = \frac{2.642\,62 \times 10^{-11}(n[\text{cm}^{-3}]/\nu)^{2/3}}{m_{de}(\chi/\chi_0)} s. \tag{9}$$

IV. RESULTS AND DISCUSSION

We compare obtained theoretical and experimental results in Figs. 3–5. The spin-susceptibility enhancement-factor (χ/χ_0) and effective mass (m_{de}) were adjusted[35] to optimize the fit between theoretical and experimental curves; note, however, that this adjustment does not affect our main picture, with negative values for the magnetoresistivity as well as its signal inversion. In Fig. 3, we show the results for the sample with the lowest doping concentration, which is closest to the metal–nonmetal transition (reminding that[36] $n_c \approx 2.5 \times 10^{17}\,\text{cm}^{-3}$) and for which the magnetoresistance presents a minimum that becomes deeper when the temperature

Published under license by AIP Publishing.

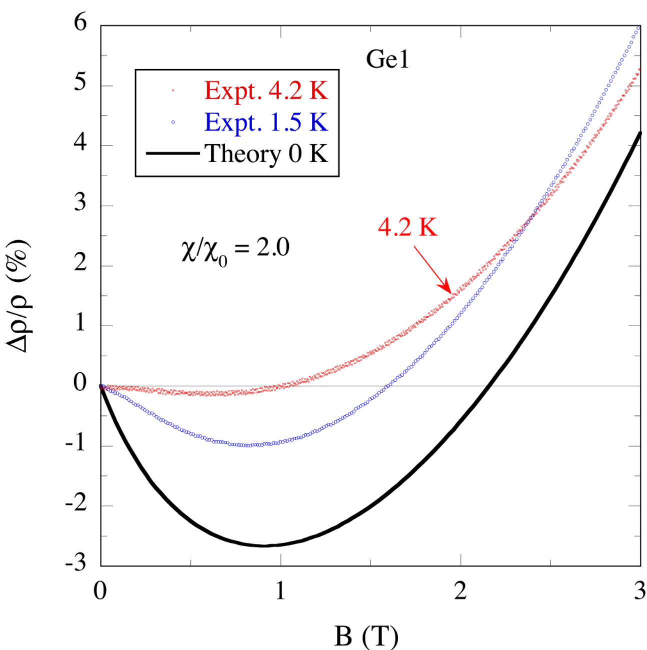

FIG. 3. The magnetoresistance at the temperatures 4.2 K (red curve) and 1.5 K (blue curve) as a function of magnetic induction, B, for a Ge:P sample with a doping concentration of 2.96×10^{17} cm^{-3}. The black solid curve is our theoretical result for 0 K. See the text for details.

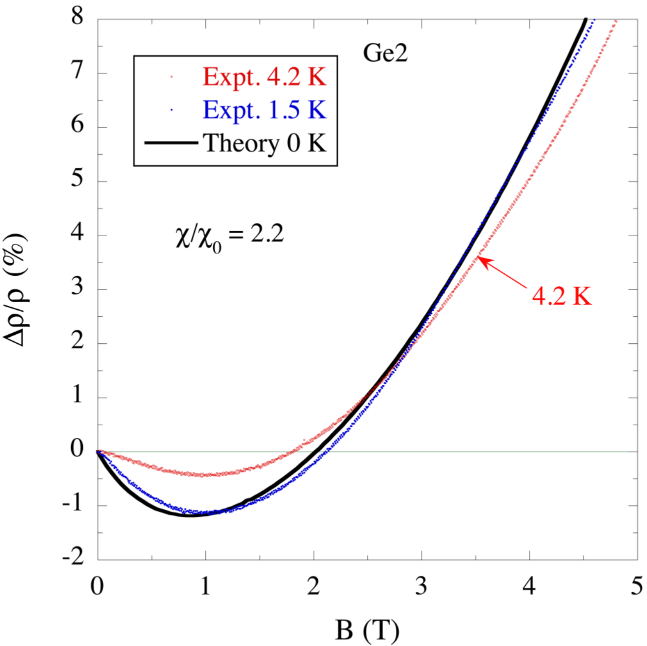

FIG. 4. The same as Fig. 3, but here for the doping concentration of 6.25×10^{17} cm^{-3}.

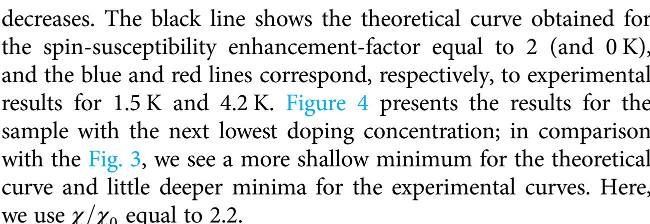

decreases. The black line shows the theoretical curve obtained for the spin-susceptibility enhancement-factor equal to 2 (and 0 K), and the blue and red lines correspond, respectively, to experimental results for 1.5 K and 4.2 K. Figure 4 presents the results for the sample with the next lowest doping concentration; in comparison with the Fig. 3, we see a more shallow minimum for the theoretical curve and little deeper minima for the experimental curves. Here, we use χ/χ_0 equal to 2.2.

In Fig. 5, we present the results for the sample with the highest doping concentration, where we use χ/χ_0 equal to 2.5. In this figure, the relatively high noise level is related to increased digital noise level due to a larger dynamic range used in lock-in amplification compared with measurements in Figs. 3 and 4. Analyzing Figs. 3–5, we identify two competing effects: while the lowering of the doping density leads to deeper minima, the increment of the temperature leads to shallower minima. It is also important to note that, near and on the metallic side of the metal–nonmetal transition, the enhancement of the density of states at the Fermi level increases. Furthermore, the enhancement of the spin susceptibility also increases when the density comes closer to n_c; however, it is reduced when the temperature goes up.[11,12,37,38] Using a log–log plot, in Fig. 6, we show how the maximum negative magnetoresistance decreases linearly when the doping concentration increases. Note that the maximum starts to decrease at a density that depends on the temperature. The higher the temperature, the earlier the maximum starts to decrease, as also reported in Ref. 13.

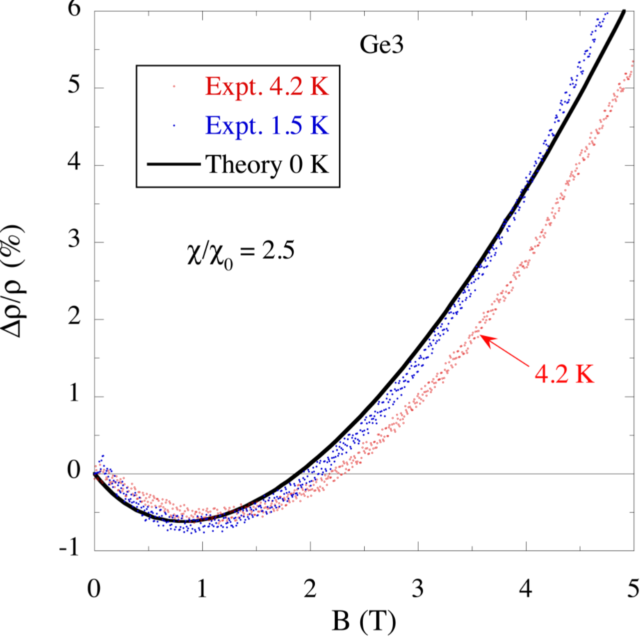

FIG. 5. The same as Fig. 3, but here for the doping concentration of 1.17×10^{18} cm^{-3}.

Published under license by AIP Publishing.

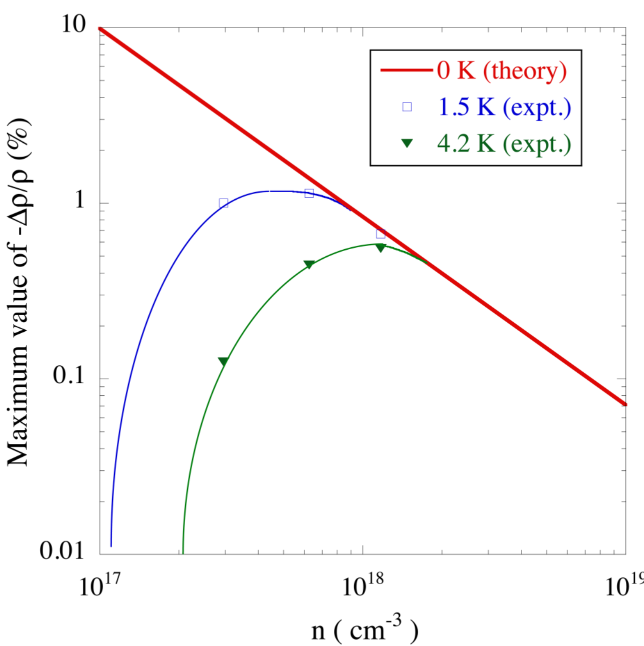

FIG. 6. The depth of the magnetoresistance minima as a function of doping concentration. The *red* thick solid straight line is the theoretical result for 0 K; the *blue* open squares are the experimental results at 4.2 K; the *green* filled triangles are the experimental results for 1.5 K; the thin solid curves are just guides for the eye. See the text for details.

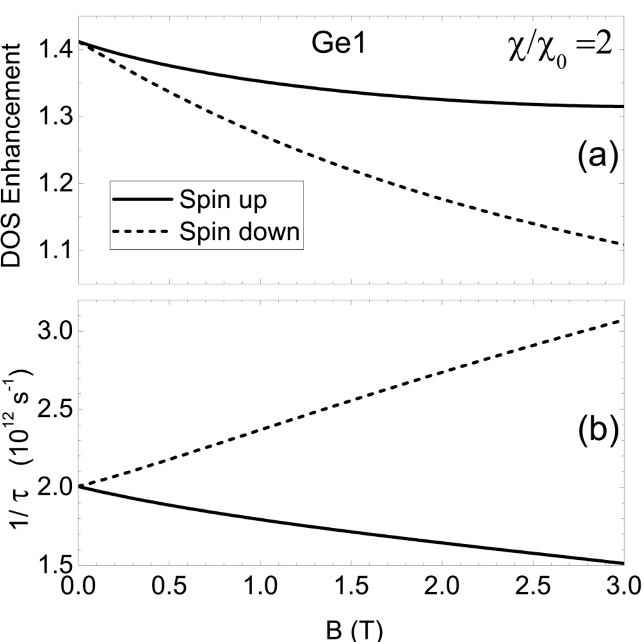

FIG. 7. (a) The enhancement of the density of states at the Fermi level for spin-up and spin-down electrons as functions of the magnetic induction B. (b) The inverse transport time for spin-up and spin-down electrons as functions of B. In (a) and (b), we consider the doping concentration of $2.96 \times 10^{17}\ \mathrm{cm}^{-3}$.

Here, we propose an explanation to the cause of the negative magnetoresistance observed at low temperatures in heavily phosphorous doped germanium on the metallic side of the metal–nonmetal transition. First, in the absence of magnetic fields, the density-of-states enhancement at the Fermi level contributes to the enhanced resistivity. Second, the presence of a magnetic field lifts the degeneracy of the electron dispersion, resulting in an upshifted spin-up band and a downshifted spin-down band. At the Fermi level, there is a redistribution of electrons between spin-up and spin-down bands, which leads spin-up and spin-down electrons to states with wave-numbers $k_0{}^{\uparrow}$ and $k_0{}^{\downarrow}$, respectively. Consequently, the peak corresponding to the density of states at the Fermi-level splits into $k_0{}^{\uparrow}$ and $k_0{}^{\downarrow}$: for electrons with $k_0{}^{\uparrow}$, one peak remains at the Fermi-level while the other moves down into the unoccupied part of the bands; instead, for electrons with $k_0{}^{\downarrow}$, while one peak remains at the Fermi-level, the other moves up into the occupied part of the bands. The enhancement at the Fermi-level is, then, reduced for both spin types.

In Fig. 7(a), we show the enhancement of the density of states at the Fermi-level, for both spin up and spin down, as functions of the magnetic-field modulus, considering the lowest doping concentration (i.e., $2.96 \times 10^{17}\ \mathrm{cm}^{-3}$). We are also considering that only the enhancement at the Fermi level affects the resistivity and that the effect due to the scattering against Friedel oscillations,[39] which eventually contributes to the enhancement of the resistivity,[29] can be negligible in heavily n-doped Ge. For completeness, we show in Fig. 7(b) how the scattering rates for spin-up and spin-down electrons vary with the magnetic-field modulus.

Our model considers the temperature equal to zero, but the knowledge acquired from experiments shows that the magnetoresistance reduces when the temperature increases.[13] To interpret this well-known behavior, note that the peak of the density of states at the Fermi-level is expected to be broadened and only states at the Fermi-level contribute to the conductivity, at zero temperature. The temperature effect enables states away from the Fermi-level, for which enhancement of the density of states is weaker, to contribute to the conductivity, and we expect that these effects gradually remove the negative magnetoresistance (reminding that temperature effects become more important for lower densities, as can be seen in our experimental results as well as in Ref. 13). Furthermore, beyond the generalized Drude model, transport anomalies also can be analyzed, for example, within a band structure approach.[40,41]

V. CONCLUSIONS

To summarize and conclude, we have investigated the anomalous regime of the longitudinal magnetoresistance of heavily n-doped germanium on the metallic side of the metal–nonmetal transition, by using magnetotransport measurements at low temperatures (1.5 K and 4.2 K) and comparing with obtained results from the many-body theory, where the donor electrons are assumed to reside at the bottom of the many-valley conduction band of the host. For doping densities above and close to n_c, we found a regime

Published under license by AIP Publishing.

formed by negative values of the magnetoresistance that is drastically suppressed when the temperature increases and physically interpreted in terms of the many-body effects. The obtained results show that the experiments support the model and can help in understanding the mechanism of magnetoresistance of heavily doped semiconductors. Besides, the presented results open the possibility to explore the interplay with other relevant conduction/resistance mechanisms at low temperatures, like the weak localization. Additionally, more samples in the doping range of 10^{18}–10^{19} cm^{-3} would be helpful for further verification of the theory.

ACKNOWLEDGMENTS

The authors acknowledge financial support from the Brazilian agencies: CNPq (Project No. 303304/2010-3), CAPES (No. PNPD 88882.306206/2018-01), FAPESB (Nos. PNX 0007/2011 and INT 0003/2015), and FAPESP (Project No. 15/16191-5).

REFERENCES

[1] W. Shockley, Bell Syst. Tech. J. **28**, 435 (1949).
[2] D. M. Chapin, C. S. Fuller, and G. L. Pearson, J. Appl. Phys. **25**, 676 (1954).
[3] J. Frigerio *et al.*, Phys. Rev. B **94**, 085202 (2016).
[4] B. E. Sernelius, K.-F. Berggren, Z.-C. Jin, I. Hamberg, and C. G. Granqvist, Phys. Rev. B **37**, 10244 (1988).
[5] I. Hamberg, C. G. Granqvist, K.-F. Berggren, B. E. Sernelius, and L. Engström, Phys. Rev. B **30**, 3240 (1984).
[6] B. I. Shklovskii and A. L. Efros, *Electronic Properties of Doped Semiconductors* (Springer, Berlin, 1984).
[7] M. Cuevas and H. Fritsche, Phys. Rev. **137**, A1847 (1965).
[8] B. E. Sernelius, Phys. Rev. B **27**, 6234 (1983).
[9] A. Feldman, Phys. Rev. **150**, 748 (1966).
[10] N. Kobayashi, S. Ikehata, S. Kobayashi, and W. Sasaki, Solid State Commun. **24**, 67 (1977).
[11] J. D. Quirt and J. R. Marko, Phys. Rev. Lett. **26**, 318 (1971).
[12] J. D. Quirt and J. R. Marko, Phys. Rev. B **5**, 1716 (1972).
[13] C. Yamanouchi, K. Miziguchi, and W. Sasaki, J. Phys. Soc. Jpn. **22**, 859 (1967) and references therein.
[14] W. Sasaki, J. Phys. Soc. Jpn. **21**, 543 (1966).
[15] A. N. Ionov, I. S. Shlimak, and A. L. Efros, Fiz. Tverd. Tela. **17**, 2763 (1975); Sov. Phys. Solid State **17**, 1835 (1976).
[16] D. G. Andrianov, G. U. Lazareva, A. S. Savel'ev, and V. I. Fistul', Fiz. Tekh. Poluprovodn. **9**, 210 (1974); Sov. Phys. Semicond. **9**, 141 (1975).
[17] E. I. Zavitskaya, I. D. Voronova, and N. V. Roshdestvenskaya, Fiz. Tekh. Poluprovodn. **6**, 1945 (1972); Sov. Phys. Semicond. **6**, 1668 (1973).
[18] O. V. Emel'yanenko, T. S. Lagunova, K. G. Masagutov, D. N. Nasledov, and D. D. Nedeoglo, Fiz. Tekh. Poluprovodn. **9**, 1517 (1975); Sov. Phys. Semicond. **9**, 1001 (1976).
[19] S. Ishida and E. Otsuka, J. Phys. Soc. Jpn. **42**, 542 (1977).
[20] B. P. Khosla and J. R. Fisher, Phys. Rev. B **2**, 4084 (1970).
[21] Y. Toyozawa, J. Phys. Soc. Jpn. **17**, 986 (1962).
[22] M. N. Alexander and D. F. Holcomb, Rev. Mod. Phys. **40**, 815 (1968).
[23] B. E. Sernelius and K.-F. Berggren, Philos. Mag. **43**, 115 (1981).
[24] G. D. Mahan, *Many-Particle Physics*, 3rd ed. (Plenum-Kluwer, New York, 2000).
[25] J. F. Ziegler, J. P. Biersak, and U. Littmark, *The Stopping and Range of Ion in Solids* (Pergamon, New York, 1985), Vol. I.
[26] L. J. Van der Pauw, Philips Res. Rep. **13**, 1 (1958).
[27] A. Ferreira da Silva, B. E. Sernelius, J. P. de Souza, H. Boudinov, H. Zheng, and M. P. Sarachik, Phys. Rev. B **60**, 15824 (1999).
[28] E. Abramof, A. Ferreira da Silva, B. E. Sernelius, J. P. de Souza, and H. Boudinov, Phys. Rev. B **55**, 9584 (1997).
[29] A. Ferreira da Silva, A. Levine, Z. S. Momtaz, H. Boudinov, and B. E. Sernelius, Phys. Rev. B **91**, 214414 (2015).
[30] B. E. Sernelius and K.-F. Berggren, Phys. Rev. B **19**, 6390 (1979).
[31] B. E. Sernelius, Phys. Rev. B **41**, 3060 (1990).
[32] B. E. Sernelius, Phys. Rev. B **40**, 12438 (1989).
[33] B. E. Sernelius, Phys. Rev. B **43**, 7136 (1991).
[34] J. M. Ziman, Philos. Mag. **6**, 1013 (1961).
[35] We have enhanced the effective mass, m_{de}, characterizing the Fermi spheres with a factor of 1.5, i.e., it has been changed from 0.22 to 0.33. Also note that the adjustment of χ/χ_0 only affects the theoretical curves in the horizontal direction.
[36] N. F. Mott, *Metal-Insulator Transitions* (Taylor and Frances, London, 1974).
[37] J. D. Quirt and J. R. Marco, Phys. Rev. B **7**, 3842 (1973).
[38] A. Ferreira da Silva, Phys. Rev. B **38**, 10 (1988). 055.
[39] J. Friedel, Nuovo Cimento Suppl. **7**, 287 (1958).
[40] P. P. Altermatt, A. Schenk, and G. Heiser, J. Appl. Phys. **100**, 113714 (2006).
[41] P. P. Altermatt, A. Schenk, B. Schmithüsen, and G. Heiser, J. Appl. Phys. **100**, 113715 (2006).

Published under license by AIP Publishing.